THE JOURNAL OF BIOLOGICAL CHEMISTRY VOL. 286, NO. 14, pp. 12149–12156, April 8, 2011

Globular Domain of the Prion Protein Needs to Be Unlocked by Domain Swapping to Support Prion Protein Conversion*[S]

Received for publication, December 18, 2010, and in revised form, February 10, 2011 Published, JBC Papers in Press, February 15, 2011, DOI 10.1074/jbc.M110.213926

Iva Hafner-Bratkovič[‡], Romina Bester[§], Primož Pristovšek[‡], Lars Gaedtke[§], Peter Veranič[¶], Jernej Gašperšič[‡], Mateja Manček-Keber[‡], Matevž Avbelj[‡], Magdalini Polymenidou[‖1], Christian Julius[‖], Adriano Aguzzi[‖2], Ina Vorberg[§3], and Roman Jerala[‡‡‡4]**

*From the [‡]Department of Biotechnology, National Institute of Chemistry, Hajdrihova 19, 1000 Ljubljana, Slovenia, the [§]Institute of Virology, Technical University Munich, Trogerstrasse 30, 81675 München, Germany, the [¶]University of Ljubljana, School of Medicine, Institute of Cell Biology, Lipičeva 2, 1000 Ljubljana, Slovenia, the [‖]Institute of Neuropathology, University Hospital Zurich, Schmelzbergstrasse 12, 8091 Zurich, Switzerland, the **Faculty of Chemistry and Chemical Technology, University of Ljubljana, Aškerčeva 5, Slovenia, and [‡‡]EN→FIST Centre of Excellence, Hajdrihova 19, 1000 Ljubljana, Slovenia*

Prion diseases are fatal transmissible neurodegenerative diseases affecting many mammalian species. The normal prion protein (PrP) converts into a pathological aggregated form, PrP^{Sc}, which is enriched in the β-sheet structure. Although the high resolution structure of the normal PrP was determined, the structure of the converted form of PrP remains inaccessible to high resolution techniques. To map the PrP conversion process we introduced disulfide bridges into different positions within the globular domain of PrP, tethering selected secondary structure elements. The majority of tethered PrP mutants exhibited increased thermodynamic stability, nevertheless, they converted efficiently. Only the disulfides that tether subdomain B1-H1-B2 to subdomain H2-H3 prevented PrP conversion *in vitro* and in prion-infected cell cultures. Reduction of disulfides recovered the ability of these mutants to convert, demonstrating that the separation of subdomains is an essential step in conversion. Formation of disulfide-linked proteinase K-resistant dimers in fibrils composed of a pair of single cysteine mutants supports the model based on domain-swapped dimers as the building blocks of prion fibrils. In contrast to previously proposed structural models of PrP^{Sc} suggesting conversion of large secondary structural segments, we provide evidence for the conservation of secondary structural elements of the globular domain upon PrP conversion. Previous studies already showed that dimerization is the rate-limiting step in PrP conversion. We show that separation and swapping of subdomains of the globular domain is necessary for conversion. Therefore, we propose that the domain-swapped dimer of PrP precedes amyloid formation and represents a potential target for therapeutic intervention.

Prion diseases, also called transmissible spongiform encephalopathies, are neurodegenerative diseases affecting a variety of mammalian species from mink to cow, with human being no exception. In these diseases, cellular prion protein (PrP^{C})[5] converts into the aggregated form PrP^{Sc}, which is the main component of the infectious agents, the prions (1). PrP^{C} is a glycosylphosphatidylinositol-anchored protein found on the membranes of neurons and many other cells (2). The N-terminal half of the protein, which is devoid of a defined tertiary structure (3), is followed by a C-terminal globular domain composed of three α-helices (H1, H2, H3) and a short antiparallel β-sheet (composed of two strands, B1 and B2) (Fig. 1*A*) (4). High resolution structures of the C-terminal domain of PrP from different species revealed the conservation of the protein fold (5). In contrast to the availability of structural information on PrP^{C}, the characteristics of PrP^{Sc} make it inaccessible to high-resolution structural techniques (x-ray crystallography and high resolution NMR). PrP^{Sc} is characterized by the increased content of the β-secondary structure in comparison to PrP^{C} (6–8). Epitope accessibility (9–12), deuterium exchange (13–15), limited proteolysis and mass spectrometry (16) studies revealed differences in surface exposure between PrP^{Sc} and PrP^{C}. Based on electron microscopy of two-dimensional crystals of a truncated form of PrP^{Sc}, Wille *et al.* (17) proposed a β-helix model of PrP^{Sc}. In this model, only the C-terminal part of H2 and H3 are conserved, whereas the majority of the remaining PrP forms a β-helix. A spiral model using molecular dynamics simulations was proposed based on the same experimental data predicting that all three helices are conserved, but that an additional β-strand is formed in the loop between B1 and H1 (18, 19). In contrast to those two models, the major structural transformation was also predicted in the region of B2, H2, and H3 and connecting segments (13). This region was proposed to form a single molecule extended layer (20). Several

* This work was supported by grants from the Slovenian Research Agency (to I. H.-B. and R. J.), EN-FIST Centre of Excellence (to R. J.), Sonderforschungsbereich 597 B14 (to I. V.), the 6th framework European Union project, TSEUR (to A. A., R. J., and I. V.), the Novartis Research Foundation (to A. A.), and the Swiss National Foundation (to A. A.).

[S] The on-line version of this article (available at http://www.jbc.org) contains supplemental Figs. S1–S9.

[1] Present address: Dept. of Cellular and Molecular Medicine, University of California, San Diego, 9500 Gilman Dr., La Jolla, CA 92093-0670.

[2] Recipient of an Advanced Grant of the European Research Council.

[3] Present address: German Centre for Neurodegenerative Diseases (DZNE), Ludwig-Erhard-Allee 2, 53175 Bonn, Germany.

[4] To whom correspondence should be addressed: Dept. of Biotechnology, National Institute of Chemistry, Hajdrihova 19, SI-1000 Ljubljana, Slovenia. Tel.: 38614760335; Fax: 38614760300; E-mail: roman.jerala@ki.si.

[5] The abbreviations used are: PrP, prion protein; mPrP, murine prion protein; PK, proteinase K; GdnHCl, guanidine hydrochloride; TEM, transmission electron microscope.

such layers stack on top of each other forming a parallel, in-register β-structure (20), which could also be supported by the solid state NMR studies (21). Relevance of the *in vitro* conversion studies of the recombinant PrP was confirmed by the demonstration of infectivity of *in vitro* converted PrP (22–25).

To map the PrP segments that participate in structural transition, we decided to design additional disulfide tethers into the globular domain of murine PrP (mPrP). Most of the PrP disulfide mutants were more stable than the wild-type protein, however, the stability did not correlate with their conversion propensity. Our results reveal that disulfide tethering of most of the secondary structural elements does not inhibit conversion, suggesting that the majority of the PrP secondary structural elements and their arrangement are conserved upon structural transition. Fibrillization results show that only covalent tethering of subdomain A (B1-H1-B2) to subdomain B (H2-H3) aborts fibrillization, demonstrating that separation of the two subdomains is a necessary step for the conversion. Our results are further supported by selective conversion of disulfide mutants in cell culture and by the fibrillization of mutants with two additional disulfide bonds. By engineering single cysteine mutants we show that a domain-swapped dimer is a building block of PrP fibrils.

EXPERIMENTAL PROCEDURES

Materials—3F4 antibodies were purchased from Dako, Cy2-conjugated anti-mouse antibodies from Dianova, goat anti-mouse HRP-conjugated antibodies from Jackson ImmunoResearch, and nickel-nitrilotriacetic acid resin from Qiagen. TEM grids were from SPI Supplies, mica from Ted Pella, AFM probes from NanoWorld, GdnHCl and urea were purchased from Fluka, cell culture media and chemicals were from Invitrogen. All other chemicals were purchased from Sigma.

Selection of Possible Sites for Additional Disulfide Formation and Molecular Modeling—Most of the designed disulfide bridges were determined by analysis of structures of recombinant prion proteins, especially mPrP structure 1AG2 (26) using MODIP (Modeling of Disulfide bridges in Proteins) (27).

The coordinates of two adjacent PrP molecules A and B, each derived from PDB entry 1XYX (28), were used to prepare the initial switched dimer model; the first switched dimer model D1 consisted of coordinates of residues 121–162 from molecule A and 172–232 from molecule B, whereas the second switched dimer model D2 consisted of coordinates of residues 121–162 from molecule B and 172–232 from molecule A. The connecting residues 163–171 for each molecule D1 and D2 were modeled using the program Modeler (29); different initial orientations and separations of two adjacent PrP molecules A and B were used. Swapped dimers of PrP were docked using the Gramm algorithm, based on smoothed potentials, refinement stage, and knowledge-based scoring (30).

Preparation of PrP Disulfide Mutant Constructs—For expression in *Escherichia coli*, pairs of cysteines were introduced into the 3F4-tagged mPrP (L108M, V111M) open reading frame (from residues 23 to 230) cloned into plasmid pRSET A using the QuikChange kit. Pairs of cysteines corresponding to mutants CC7 and CC9 were also introduced into the 3F4-tagged mPrP open reading frame in pcDNA3.1zeo(+) by site-directed mutagenesis and these open reading frames were further subcloned into retroviral expression vector pSFF (31–33). The 3F4 tag was used to facilitate detection by 3F4 antibody and distinguish it from endogenous mPrP in infected cell lines.

Protein Expression, Purification, and Refolding—Plasmid pRSET A encoding mPrP mutants was transformed into competent *E. coli* BL21(DE3) pLysS. The protein was purified from inclusion bodies and refolded on a nickel-nitrilotriacetic acid column using a previously described protocol (34–36). The purity of mutant isolates was checked by SDS-PAGE. Disulfide formation was confirmed by mass spectrometry.

Circular Dichroism Spectroscopy—Circular dichroism spectra were recorded on an Applied Photophysics Chirascan spectropolarimeter. Far-UV CD spectra were recorded between 190 and 250 nm in a 1-mm path length cuvette at a protein concentration of 0.1 mg/ml. The thermal stability of proteins was recorded in a 1-mm path length cuvette at protein concentrations of 0.1 mg/ml with a temperature scan rate of 1 °C/min at 222 nm.

Conversion to the Fibrillar Form of the Prion Protein—A conversion reaction adopted from Bocharova *et al.* (37) was used for tracking the fibrillization of PrP disulfide mutants. Correctly folded proteins were first denatured in 6 M GdnHCl. The amyloid forms were produced by diluting denatured WT and mutants into 1 M GdnHCl, 3 M urea, phosphate-buffered saline, pH 6.8, at protein concentrations of 22 μM and shaking at 37 °C (37).

Thioflavin T Fluorescence—A PerkinElmer LS55 fluorimeter was used for fluorescence measurements. Thioflavin T emission (460–535 nm) was tracked by excitation at 442 nm at protein concentrations of 1 and 5 μM thioflavin T.

Transmission Electron Microscopy—After conversion the reaction mixtures were adsorbed to poly-L-lysine-coated holey formvar carbon-coated copper grids for 3 min, negatively stained with 1% (w/v) aqueous uranyl acetate for 1.5 min, and observed under a Jeol 100CX electron microscope operating at 80 keV as previously described (35).

Atomic Force Microscopy—A drop of PrP (0.22 μM) was applied to freshly cleaved mica and left to adsorb for 5 min after which it was washed twice with filtered Milli-Q water and dried under the stream of nitrogen. Samples were observed by Agilent Technologies 5500 Scanning Probe Microscope operating in acoustic alternating current mode utilizing silicon cantilevers (Arrow-NCR) with a force constant of 42 newton/m.

Indirect ELISA Using POM Antibodies—Wild-type PrP and PrP disulfide mutants in native and amyloid forms were coated into maxisorp microtiter plates (Nunc) at various concentrations. After protein adsorption, wells were blocked by 1% BSA. Anti-PrP antibodies of the POM panel (38), POM1 (7.5 ng/ml), POM2 (4.8 ng/ml), POM3 (15 ng/ml), POM4 (10 ng/ml), and POM5 (15 ng/ml), were added. After washing, goat anti-mouse HRP-conjugated antibodies were added and absorbance (at 405 nm) was detected after the addition of ABTS (2,2-azino-bis(3-ethylbenzothiazoleline-6-sulfonic acid) substrate.

Conversion and Analysis of Single Cysteine Mutants M133C and Q216C—Fibrillization was initiated by diluting WT and single cysteine mutants into 1 M GdnHCl, 3 M urea, phosphate-

buffered saline, pH 6.8, at total protein concentrations of 22 μM and shaking at 37 °C. The molar ratio of M133C and Q216C was 1:1 (11 μM of each mutant). Fibrillization reactions were diluted with 0.1 M Tris buffer, pH 7.5, and subjected to different proteinase K:PrP ratios for 45 min at 37 °C. The digestion was stopped with 5 mM PMSF. Proteins were precipitated by methanol and solubilized in denaturing sample buffer with or without β-mercaptoethanol (39). Detection of prion protein-specific bands was achieved by POM1 antibody (1:4000).

Production of Retrovirions and Transduction of HpL3-4 and L929/22L Cell Lines—The pSFF vectors were transfected into co-cultures of packaging cell lines ψ2 and PA317. When cells were more than 80% positive for prion protein, retroviral supernatants were harvested and cleared by centrifugation (120 × *g*, 4 °C, 10 min). 3×10^5 cells per well of HpL3-4 (40) or L929 cells persistently infected with prion strain 22L (41) were plated 1 day before transduction into 6-well plates. Cells were incubated with Polybrene (4 μg/ml) 2 h before addition of retrovirions. 1 ml of retroviral supernatant was incubated with the cells for 2 days, after which the cells were transferred into a 6- or 10-cm culture plate.

Flow Cytometry—We used a flow cytometry protocol adapted from Maas *et al.* (42) to check whether PrP disulfide mutants are expressed at the cell surface of HpL3-4 cells similarly to the wild-type PrP. 5×10^5 cells were first incubated with FACS buffer (2.5% FCS in PBS) for 10 min at 4 °C. 100 μl of 3F4 antibody (5 μg/ml) was added to the cells and incubated for 45 min at 4 °C. After washing, the cells were incubated with Cy2-conjugated anti-mouse secondary antibodies for 45 min at 4 °C in the dark. The rinsed cells were analyzed by flow cytometry.

Infection of HpL3-4—A day before infection 5×10^4 cells were seeded into each well of a 24-well microtiter plate. 200 μl of DMEM supplemented with 10% serum and 1% 22L-positive brain homogenate were added to the cells and incubated for 4 h. After this incubation 400 μl of growth medium was added and the cells were left to grow to near confluence when the cells were moved stepwise into 6- and 9-cm Petri dishes (41, 42).

Analysis of Protease-resistant PrP—Infected Hpl3-4 and transduced L929/22L cells were washed and lysed. 1/10 of the sample was methanol precipitated and used for determination of the total amount of PrP. The rest of the sample was incubated with proteinase K (20 μg/ml) at 37 °C for 30 min when the proteinase digestion was stopped by the addition of Pefabloc and ultracentrifuged. Pellets were resuspended in SDS-sample buffer and analyzed by Western blot. A 3F4 antibody was used for the detection of the conversion of mutant proteins (transduced 3F4-tagged wild-type mPrP, CC7, and CC9) and a 4H11 antibody (43) was used for the detection of endogenous and mutant proteins.

RESULTS

Engineering of Additional Disulfides into the mPrP Structure—To map the PrP^C to PrP^{Sc} conversion we designed nine additional disulfide bridges into the globular domain of mouse PrP (Fig. 1*B*). All sites matched steric criteria favoring disulfide formation (27) and were chosen to tether different secondary structural elements of the globular domain of mPrP. PrP disulfide mutants CC1, CC3, and CC5 had disulfides introduced within the B1-H1-B2 segment, with CC1 enclosing the longest and CC5 enclosing the shortest segment (Fig. 1*B*). The H2-H3 region, which is already connected by a native disulfide was also tethered by additional disulfides in CC8 and CC9 mutants. Disulfides tethering the longest polypeptide segment belonged to CC2 and CC4, where the B1-H1-B2 region was tethered to H3, and CC7 connecting B2 to H3. We were able to purify and refold seven PrP disulfide mutants (supplemental Fig. S1). As the wild-type PrP (WT), all refolded mutants had a high content of α-helical structure, characterized by two minima in the far-UV CD spectrum (supplemental Fig. S2*A*). We were unable to refold mutants CC6 and CC8, probably due to the proximity of the native and engineered cysteines. Although the majority of additional disulfides increased protein stability (Table 1 and

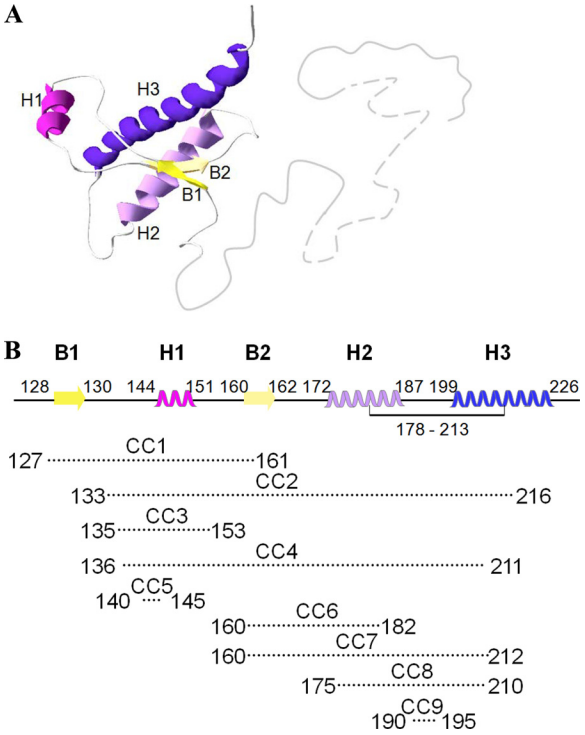

FIGURE 1. **Scheme of sites for additional disulfide formation.** *A*, mouse prion protein is composed of a N-terminal unfolded part (*gray line*) and a globular domain, which consists of α-helices H1, H2, and H3 and an antiparallel β-sheet (B1 and B2) (PDB 1XYX (28)). *Dashed line* in the unfolded N-terminal part represents the octarepeat region. *B*, below representation of the secondary structural elements, the *dotted lines* connect the positions of engineered disulfides in PrP disulfide mutants. The native disulfide bridge connects amino acid residues 178 and 213 and is drawn as a *solid line*. Mouse PrP numbering is used.

TABLE 1

Thermal stability of PrP disulfide mutants

Thermal stability of PrP mutants was determined from circular dichroism at 222 nm. The engineered disulfide bridge increases stability of the majority of PrP disulfide mutants in comparison to WT. For the most stable mutants only the lower limit is indicated, as the T_m could not be calculated accurately.

Protein	No. of amino acid residues enclosed	T_m
		°C
WT		63.5 ± 0.2
CC1	35	66.6 ± 0.1
CC2	84	>75
CC3	19	>76
CC4	76	>72
CC5	5	57.9 ± 0.2
CC7	53	69.7 ± 0.4
CC9	6	70.5 ± 0.1

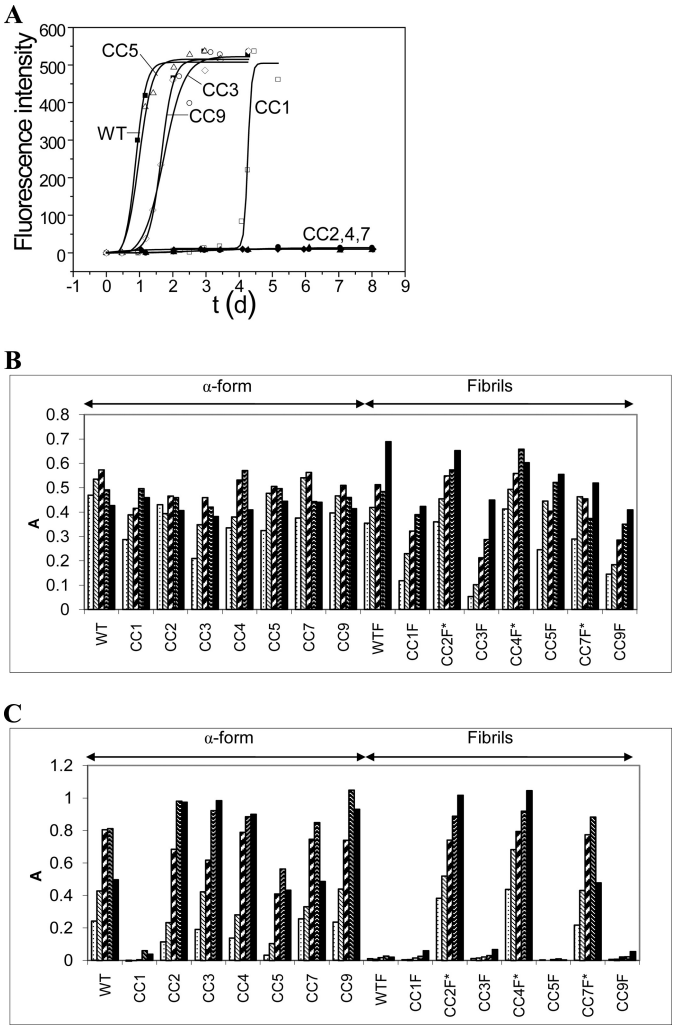

FIGURE 2. ***In vitro* conversion of PrP disulfide mutants.** *A*, fluorescence emission of the amyloid-specific dye thioflavin T at 482 nm was used to follow the time course of the conversion of PrP disulfide mutants CC1 (□), CC2 (●), CC3 (○), CC4 (▲), CC5 (△), CC7 (♦), CC9 (◇), and WT (■) *in vitro*. A representative of four experiments is shown. *B*, binding of mAb POM2 recognizing the epitope in the octarepeat region in the N-terminal unstructured part of PrP to the native α-form (*left* of the chart) or fibrils (*right* of the chart). Proteins were applied to microtiter plates at protein concentrations 0.5 (▨), 1 (▧), 2 (▨), 3 (▨), and 5 μg/ml (■). In the case of non-converting mutants CC2, CC4, and CC7 the conversion reaction mixture was used (designated by *). *C*, binding of mAb POM5 to the α-form and fibrils of WT and mutants. POM5 binds to the region between B2 and H2 in the globular domain. POM5 does not bind to CC1 in any form because the Y161C substitution lies in the recognition epitope of POM5.

supplemental Fig. S2*B*), only the CC5 disulfide placed at the N terminus of H1 destabilized the mutant compared with WT by ~6 °C. Mutants CC2 and CC3, one enclosing 82 and the other enclosing 19 amino acid residues were the most stable mutants in our panel of PrP disulfide mutants. Determination of disulfide mutant stability suggests that local packing interactions affect stability rather than the length of the loop enclosed by the additional disulfide.

Fibrillization of PrP Disulfide Mutants—In vitro fibrillization enables to monitor the time course of PrP conversion by fluorescence emission of the amyloid-specific dye thioflavin T (37) (Fig. 2*A*). Conversion of the WT and CC5 mutant was detected after 12 h, followed by CC9 and CC3. Fibrillization delay of the CC1 mutant was considerably longer. In contrast, the CC2, CC4, and CC7 mutants did not fibrillize even after as much as 1 month (Fig. 2*A*). The converted mutants showed a structural transition to a conformation with increased content of the β-secondary structure, which was confirmed by CD (not shown). Fibrils of morphology similar to WT were confirmed by TEM (supplemental Fig. S3). No fibrils were detected in CC2, CC4, and CC7 samples (Fig. 3*C*, *left*). CC5, which is less stable than WT, fibrillizes with comparable kinetics to WT. Mutants CC2, CC4, and CC7, which are more stable than WT, do not convert at all. However, mutant CC3 with the highest T_m converts with only a slightly longer delay than WT. Those results show that thermal stability has less influence on conversion propensity than the structural context of each mutant.

To further characterize fibrils of different PrP disulfide mutants, we used a panel of 5 antibodies with well characterized epitopes on mouse PrP^C (38, 44). We tested recognition of PrP disulfide mutants in the native and fibrillar form. The POM2 antibody with a recognition epitope in the octarepeat region bound to both forms of all mutants (Fig. 2*B*), demonstrating that the octarepeat region is not buried in fibrils. In contrast to octarepeat-binding antibody POM2, other antibodies did not bind to the fibrillar form of mPrPs, whereas they bound well to the native α-helical form (Fig. 2*C* and supplemental Fig. S4, *A–C*). All antibodies recognized CC2, CC4, and CC7 mutants under native conditions as well as under fibrillization conditions because these mutants did not convert into fibrils but retained the α-helical structure (Fig. 2*C* and supplemental Fig. S4, *A–C*).

Reduction of Disulfide Bonds Reverts Conversion Ability to PrP Disulfide Mutants—Because even single amino acid substitutions may inhibit PrP conversion (45), we wanted to exclude the possibility that the amino acid substitutions introduced for the engineered disulfide affected the conversion process. Therefore, we prepared single cysteine mutants corresponding to point substitutions for construction of the CC2 disulfide mutant. Each of the single cysteine mutants fibrillized comparably to WT (Fig. 3*A*). To prove that the covalent tethers restrict conversion, we exposed non-converting mutants CC2, CC4, and CC7 and WT to reducing conditions prior to fibrillization to disrupt disulfide bonds. This reverted the effect of disulfide tethers in non-converting mutants and all mutants fibrillized with a delay comparable with the wild-type protein (Fig. 3, *B* and *C*). These results show that restriction of the conformational space by disulfide tethers and not an amino acid substitution *per se* is the reason for non-conversion of the selected group of PrP disulfide mutants.

PrP Conversion in Cell Culture Confirms Selective Inhibition of in Vitro Fibrillization—We wanted to test whether PrP disulfide mutants have the same conversion propensities in the living cells. We expressed the representatives of non-converting (CC7) and converting (CC9) mutants and WT mPrP by retroviral transduction into prion protein knock-out cell line HpL3-4 (40, 42). Both mutants as well as wild-type PrP were expressed at comparable amounts at the cell surface (supplemental Fig. S5*A*). HpL3-4 cells expressing CC7, CC9, and WT protein were exposed to prion strain 22L. Although wild-type mPrP and CC9 supported prion propagation, as detected by the occurrence of proteinase K-resistant PrP^{Sc}

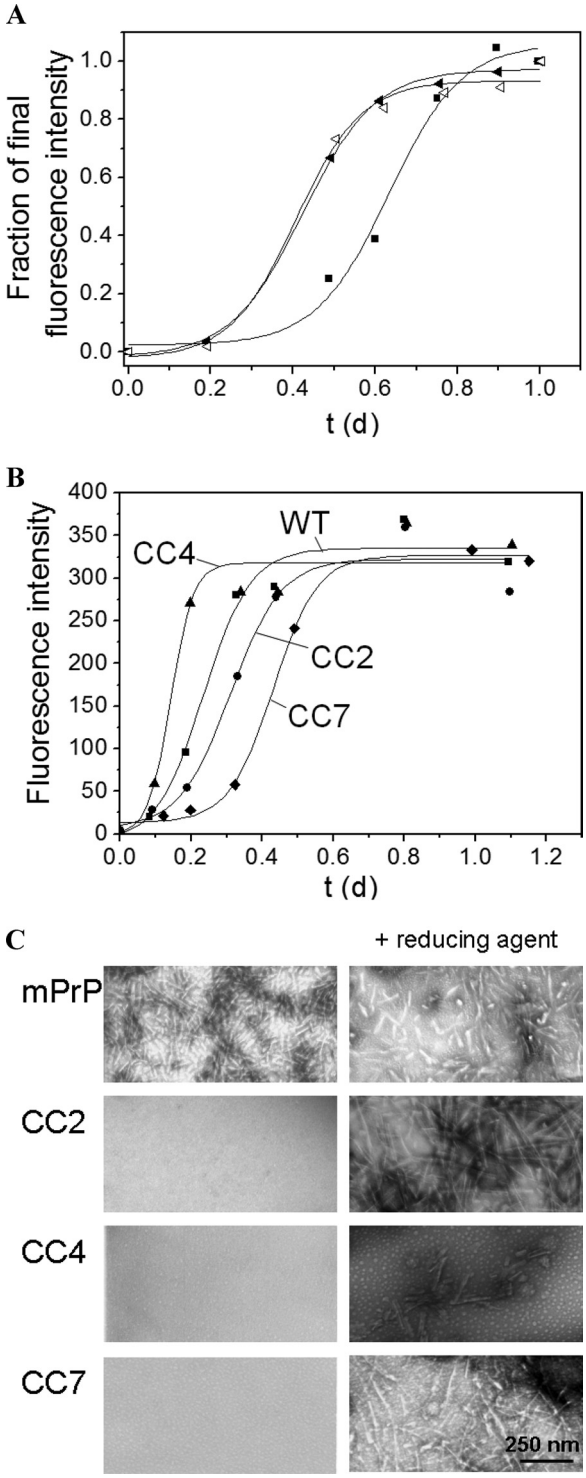

FIGURE 3. **Recovery of conversion of PrP disulfide mutants under the reducing conditions and conversion of single cysteine mutants.** *A*, fibrillization of WT (■) and single cysteine mutants of the pair of cysteines of mutant CC2: M133C (◀) and Q216C (▷). A representative of three experiments is shown. *B*, conversion of WT (■) and non-converting mutants CC2 (●), CC4 (▲), and CC7 (◆) *in vitro* in the presence of reducing agent (5 mM DTT). A representative of three experiments is shown. *C*, formation of fibrils was confirmed by transmission electron microscopy. No fibrils were observed in CC2, CC4, and CC7 samples without the reducing agent (*left*); addition of the reducing agent to the conversion reaction resulted in fibrils observed under TEM (*right*).

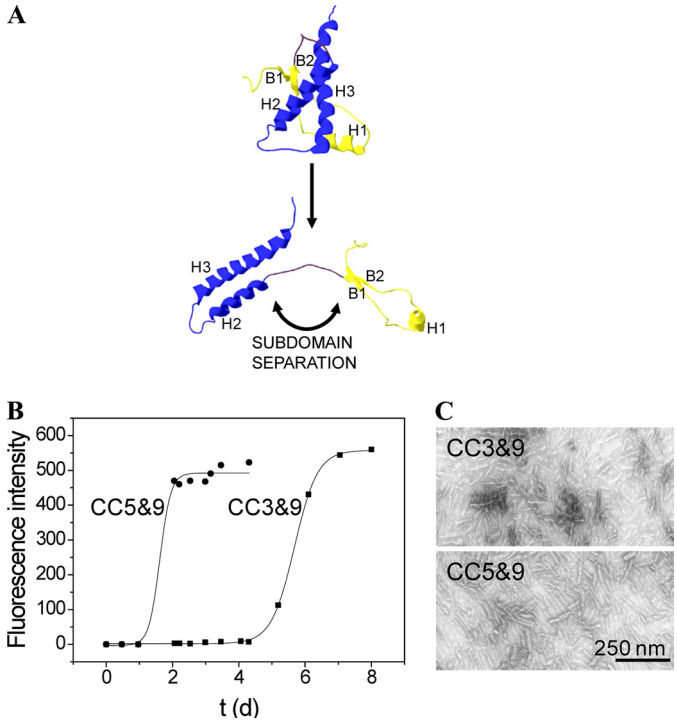

FIGURE 4. **Dissociation of subdomains in the globular domain is necessary for conversion, but is not inhibited by two additional disulfide bridges in separate subdomains of PrP.** *A*, disulfide tethers reveal the importance of the dissociation of subdomains A (*yellow*) and B (*blue*) in the conversion process. *B*, conversion of mutants with two additional disulfide bridges CC5&9 (●) and CC3&9 (■) with one disulfide bridge in subdomain A and the other in subdomain B was followed by thioflavin T emission. *C*, fibrillization of double disulfide mutants was confirmed by TEM.

(supplemental Fig. S5*B, right*), CC7 did not convert into the protease-resistant form, which is in agreement with the results of an *in vitro* assay. Additionally we were interested whether the non-converting mutant CC7 has a dominant-negative phenotype on the propagation of endogenous PrP^{Sc}. To test this we introduced WT, CC7, and CC9 mutants into cell line L929 chronically infected by prion strain 22L. All three mutants were expressed in the L929 cell line (supplemental Fig. S5*C, left*). As in the HpL3-4 cell line, the CC9 mutant was converted into a protease-resistant PrP, whereas the CC7 mutant did not (supplemental Fig. S5*C, middle*). The expression of CC7 did not affect the amount of endogenous PK-resistant PrP (supplemental Fig. S5*C, right*), from which we can conclude that CC7 does not inhibit PrP conversion.

Fibrillization of Mutants with Two Engineered Disulfide Bridges from Different Subdomains of mPrP—We can divide the C-terminal globular domain of PrP into subdomain A, consisting of secondary structural elements B1-H1-B2 and subdomain B, consisting of helices H2 and H3 (Fig. 4*A*). Converting mutants CC1, CC3, and CC5 have an additional disulfide bond in subdomain A and mutant CC9 in subdomain B. In the non-converting mutants, on the other hand, either the loop between B1 and H1 is connected to H3 (CC2 and CC4) or B2 is tethered to H3 (CC7), thereby tethering the two subdomains together.

It might be possible that the disulfide tether in one segment could be compensated by the conformational adaptation in the other subdomain. To further investigate the conservation of the secondary structure elements within the subdomains, we pro-

duced mutants with two engineered disulfide bridges, one in each subdomain. Mutant CC3&9 contains a disulfide bridge of CC3 in subdomain A and in subdomain B a disulfide corresponding to CC9. Mutant CC5&9 is tethered by a combination of CC5 disulfide in subdomain A and CC9 disulfide in subdomain B. Both mutants were correctly refolded and even though they were significantly more stable than the wild-type protein (CC5&9 had a melting temperature of 67.7 ± 0.2 °C and CC3&9 of more than 80 °C), they were, nevertheless, able to convert (Fig. 4, *B* and *C*).

We can conclude that a tether between subdomains A (B1-H1-B2) and B (H2-H3) prevents the conformational change, whereas intrasubdomain disulfide bridges allow conversion. This suggests that the conformation of each subdomain is conserved in the PrP^{Sc}, but that separation of subdomains A and B is necessary for the conversion to proceed with the loop between B2 and H2 as the pivot of conformational transition to the amyloid form (Fig. 4*A*).

Domain Swapping Is the Mechanism of PrP Conversion—Our results showing that only separation of subdomains without disruption of the existing secondary structural elements is necessary for conversion led us to propose that domain swapping is involved in the PrP conformational transition. To test this hypothesis we employed a pair of single cysteine mutants corresponding to CC2. A similar approach has been used previously to show that domain swapping is involved in fibrillization of T7 endonuclease I (46). We expected that when the M133C and Q216C mixture undergoes fibrillization, monomers form swapped dimers with either monomers of the same mutant or monomers of the other mutant. In the latter case a disulfide bond is formed between monomers only if domain swapping occurs (Fig. 5*A*). We fibrillized M133C, Q216C, and a mixture of both mutants (Fig. 5*B, right*). When fibrils were exposed to increasing concentrations of proteinase K, proteinase K-resistant dimers were observed in fibrils composed of both mutants (Fig. 5*B*, *left*). Reduction of these dimers yielded monomers, showing these dimers are covalently bound by a disulfide bridge (supplemental Fig. S6). No proteinase K-resistant dimers were observed in fibrils of separate single cysteine mutants (Fig. 5*B*, *left*) or in wild-type mPrP (supplemental Fig. S7), which, however, display similar characteristics regarding fibril formation and aggregation upon PK digestion as previously reported (37) (supplemental Fig. S8). When single cysteine mutants are exposed to mildly denaturing conditions, they are partially unfolded and a fraction of molecules form covalent dimers, which, however, do not incorporate into fibrils and are thus degraded by proteinase K (Fig. 5*B, left*, and supplemental Fig. S9).

In the molecular model of PrP conversion satisfying our disulfide constraints, subdomains A and B dissociate and interact with the corresponding subdomains of the other monomer thus forming a domain-swapped dimer (Fig. 5*C*). Because the secondary structural elements of both of the subdomains are conserved, most of the helical segments remain. However, the β-sheet content increase can arise from the conversion of the B2-H2 loop into the extended structure and particularly from ordering of the unstructured N-terminal hydrophobic region.

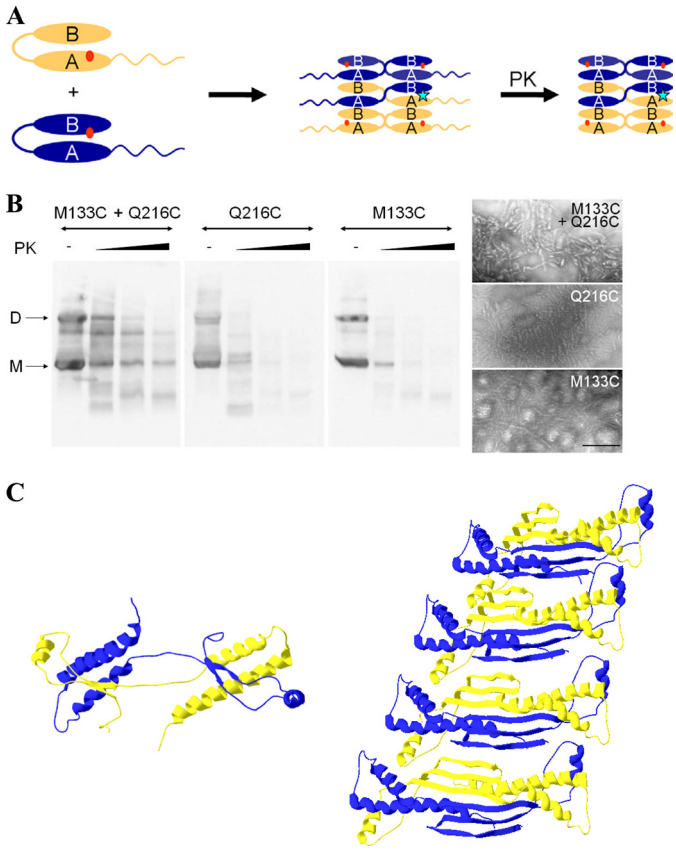

FIGURE 5. **Domain-swapped dimers are the building blocks of PrP fibrils.** *A*, schematic representation of the fibrillization experiment using a mixture of two single cysteine mutants. These cysteines could form a disulfide if they were within the same protein monomer. When one cysteine mutant monomer (*yellow*) forms a domain-swapped dimer with the other cysteine mutant monomer (*blue*), a covalent disulfide-linked dimer can be formed (disulfide bridge is depicted as a *cyan star*). Each mutant monomer can also swap the H2-H3 subdomain with the monomer of the same mutant, which, however, cannot lead to the formation of a disulfide bridge. Cysteines are depicted by *red spots*. After proteinase K digestion, the N-terminal part of the protein is partially cleaved off the fibrils. *B*, fibrillization reactions of the mixture of M133C with Q216C and each of the mutants separately were exposed to PK at PK:PrP ratios (w/w) of 1:650, 1:160, and 1:80. The *first lane* in each case is the fibrillization reaction not treated with PK. Only in the case of a M133C and Q216C mixture was a proteinase K-resistant dimer observed (bands between monomer (*M*) and dimer (*D*)). TEM images of fibrils formed by the M133C and Q216C mixture and by each mutant separately are shown on the *right*. *Bar* represents 250 nm. *C*, model of the stacking of the domain-swapped dimer units into a fibril (*right*). Dimer is formed by domain swapping of PrP, where the H2-H3 subdomain of one monomeric unit interacts with the B1-H1-B2 subdomain of the other monomeric unit (*left*). Each monomer of the domain swapped dimer is represented by a different color (*yellow* and *blue*). β-Strands annealed to the swapped dimers are formed from the disordered N-terminal segments and connect the dimer units (*right*).

DISCUSSION

The major unsolved question regarding prion diseases is the transformation of the tertiary structure of PrP, where the converted form (PrP^{Sc}) comprises the major component of the infectious particle. Results of our study reveal that a significant amount of the native-like supersecondary structure is retained in the fibrillar form of PrP, because disulfide tethers introduce very strong structural constraints that are incompatible with the major structural transformation of its secondary structural elements. Other published PrP^{Sc} models predict significant rearrangement of secondary structure elements in the globular domain. The β-helix model (17) and the spiral model (19) agree

with our results in the conservation of the major part of H2 and H3. However, the β-helix model (17) proposes that residues up to the middle of H2 change the conformation, which is incompatible with the ability of mutants CC1, CC3, and CC5 to convert. The spiral model (19) proposes an additional β-strand formation in the segment connecting B1 and H1, which would be expected to prevent conversion of mutant CC3. The models predicting major structural changes in subdomain B (20) are also not supported by our results (conversion of mutant CC9) and additionally by the presence of the native disulfide bridge. The three non-converting disulfide mutants show that in the structural conversion of PrP, subdomains A and B have to dissociate, which is also supported by a study by Eghiaian *et al.* (14) showing that connecting residues 160 and 209 in ovine PrP disabled oligomer formation.

Our molecular model of PrP^{Sc} contains 34% α-helices and 39% β-sheets, which is close to the experimentally determined secondary structure content (6–8, 47). According to this model, the main structural switch is located in the loop between B2 and H2. This region has been previously implicated in the species barrier (48) and disease resistance polymorphisms (49). NMR investigation identified differences in the structural order parameter in this region, with PrP from elk being more rigid than in other species, therefore it was called "the rigid loop" (28). Additionally, substitutions in the rigid loop led to spontaneous transmissible prion disease in transgenic mice (50).

Dimerization has been pinpointed as the rate-limiting step in PrP conversion (51) and the electron microscopy of PrP fibrils supports the dimer as the building unit of fibrils (52). A model of PrP dimer that involves ordering the 90–124 region is also in agreement with our results (53, 54). A domain swapping mechanism as the underlying motif of fibrillization has already been proposed for several amyloid-like proteins (55–57). Our non-converting mutant (CC7) failed to cure chronically infected cells, which can be explained by the inability of the mutant to sequester the wild-type mPrP into the domain-swapped dimer. Interestingly, a crystal structure of the domain-swapped PrP dimer was determined (58, 59), where H3 was involved in domain swapping. This type of crystallized dimer, however, requires disruption of the native disulfide bond, whereas previous studies have shown that the native disulfide bond is conserved upon conversion (60, 61). There is emerging evidence that polyanions such as nucleic acids and glucosaminoglycans can modulate PrP conversion (62–65). It is proposed they may act as a scaffold facilitating protein-protein interactions (64), which should augment domain-swapped dimer formation. On the other hand molecules such as heparin are effective inhibitors of PrP^{Sc} conversion (65). By binding to the globular domain (66) heparin could stabilize the PrP monomer thus inhibiting dimer formation.

Recently several prion strains were produced *in vitro*, differing primarily in fibril morphology (67, 68) and also in incubation periods in inoculated mice (68). By epitope accessibility studies using a panel of antibodies we showed that the fibrils of mutants with engineered disulfides are indistinguishable from WT fibrils. Those experiments, however, allow the possibility of different stacking of the N-terminal part preceding the globular domain. This part is not tethered by our disulfides and has been shown to differ in conformational stability among prion strains (69). Increase of the β-structure in PrP^{Sc} has been generally attributed to the conversion of α-helical segments into the β-sheet structure and different conformations of PrP were proposed to account for prion strains. However, several radically different secondary structural conformations of the same polypeptide chain are very unlikely to exist, as they would have to satisfy a large number of structural constraints simultaneously. On the contrary, it is much more likely to fold the disordered N-terminal polypeptide chain of PrP into several different β-sheet arrangements. Recently Wiltzius *et al.* (70) demonstrated that the same short peptide sequence can pack into different polymorphic β-sheets, which has been proposed as the background of the protein-encoded inheritance. Using additional disulfide bonds as tethers we were able to show that dissociation of the two subdomains, which enables swapped dimer formation, is the necessary step in the PrP structural conversion. The main role of the globular C-terminal domain in the prion protein-encoded inheritance is to act as a switch that allows annealing of the β-structure from the disordered N-terminal polypeptide segments.

Acknowledgments—We thank Darija Oven for excellent technical assistance. We are very grateful to Dr. Bogdan Kralj for mass spectrometry measurements, Dr. Suzette A. Priola and Dr. Bruce Chesebro for providing ψ2 and PA317 cells and vector pSFF, and Prof. Takashi Onodera for the HpL3-4 cells.

REFERENCES

1. Prusiner, S. B. (1998) *Proc. Natl. Acad. Sci. U.S.A.* **95,** 13363–13383
2. Harris, D. A. (1999) *Clin. Microbiol. Rev.* **12,** 429–444
3. Zahn, R., Liu, A., Lührs, T., Riek, R., von Schroetter, C., López García, F., Billeter, M., Calzolai, L., Wider, G., and Wüthrich, K. (2000) *Proc. Natl. Acad. Sci. U.S.A.* **97,** 145–150
4. Riek, R., Hornemann, S., Wider, G., Billeter, M., Glockshuber, R., and Wüthrich, K. (1996) *Nature* **382,** 180–182
5. Wüthrich, K., and Riek, R. (2001) *Adv. Protein Chem.* **57,** 55–82
6. Caughey, B. W., Dong, A., Bhat, K. S., Ernst, D., Hayes, S. F., and Caughey, W. S. (1991) *Biochemistry* **30,** 7672–7680
7. Pan, K. M., Baldwin, M., Nguyen, J., Gasset, M., Serban, A., Groth, D., Mehlhorn, I., Huang, Z., Fletterick, R. J., Cohen, F. E., *et al.* (1993) *Proc. Natl. Acad. Sci. U.S.A.* **90,** 10962–10966
8. Jackson, G. S., Hill, A. F., Joseph, C., Hosszu, L., Power, A., Waltho, J. P., Clarke, A. R., and Collinge, J. (1999) *Biochim. Biophys. Acta* **1431,** 1–13
9. Peretz, D., Williamson, R. A., Kaneko, K., Vergara, J., Leclerc, E., Schmitt-Ulms, G., Mehlhorn, I. R., Legname, G., Wormald, M. R., Rudd, P. M., Dwek, R. A., Burton, D. R., and Prusiner, S. B. (2001) *Nature* **412,** 739–743
10. Kanyo, Z. F., Pan, K. M., Williamson, R. A., Burton, D. R., Prusiner, S. B., Fletterick, R. J., and Cohen, F. E. (1999) *J. Mol. Biol.* **293,** 855–863
11. Rogers, M., Serban, D., Gyuris, T., Scott, M., Torchia, T., and Prusiner, S. B. (1991) *J. Immunol.* **147,** 3568–3574
12. Eghiaian, F., Grosclaude, J., Lesceu, S., Debey, P., Doublet, B., Tréguer, E., Rezaei, H., and Knossow, M. (2004) *Proc. Natl. Acad. Sci. U.S.A.* **101,** 10254–10259
13. Lu, X., Wintrode, P. L., and Surewicz, W. K. (2007) *Proc. Natl. Acad. Sci. U.S.A.* **104,** 1510–1515
14. Eghiaian, F., Daubenfeld, T., Quenet, Y., van Audenhaege, M., Bouin, A. P., van der Rest, G., Grosclaude, J., and Rezaei, H. (2007) *Proc. Natl. Acad. Sci. U.S.A.* **104,** 7414–7419
15. Nazabal, A., Hornemann, S., Aguzzi, A., and Zenobi, R. (2009) *J. Mass Spectrom.* **44,** 965–977
16. Sajnani, G., Pastrana, M. A., Dynin, I., Onisko, B., and Requena, J. R. (2008)

J. Mol. Biol. **382,** 88–98
17. Wille, H., Michelitsch, M. D., Guenebaut, V., Supattapone, S., Serban, A., Cohen, F. E., Agard, D. A., and Prusiner, S. B. (2002) *Proc. Natl. Acad. Sci. U.S.A.* **99,** 3563–3568
18. DeMarco, M. L., Silveira, J., Caughey, B., and Daggett, V. (2006) *Biochemistry* **45,** 15573–15582
19. DeMarco, M. L., and Daggett, V. (2004) *Proc. Natl. Acad. Sci. U.S.A.* **101,** 2293–2298
20. Cobb, N. J., Sönnichsen, F. D., McHaourab, H., and Surewicz, W. K. (2007) *Proc. Natl. Acad. Sci. U.S.A.* **104,** 18946–18951
21. Tycko, R., Savtchenko, R., Ostapchenko, V. G., Makarava, N., and Baskakov, I. V. (2010) *Biochemistry* **49,** 9488–9497
22. Legname, G., Baskakov, I. V., Nguyen, H. O., Riesner, D., Cohen, F. E., DeArmond, S. J., and Prusiner, S. B. (2004) *Science* **305,** 673–676
23. Wang, F., Wang, X., Yuan, C. G., and Ma, J. (2010) *Science* **327,** 1132–1135
24. Makarava, N., Kovacs, G. G., Bocharova, O., Savtchenko, R., Alexeeva, I., Budka, H., Rohwer, R. G., and Baskakov, I. V. (2010) *Acta Neuropathol.* **119,** 177–187
25. Kim, J. I., Cali, I., Surewicz, K., Kong, Q., Raymond, G. J., Atarashi, R., Race, B., Qing, L., Gambetti, P., Caughey, B., and Surewicz, W. K. (2010) *J. Biol. Chem.* **285,** 14083–14087
26. Glockshuber, R., Hornemann, S., Riek, R., Wider, G., Billeter, M., and Wüthrich, K. (1997) *Trends Biochem. Sci.* **22,** 241–242
27. Dani, V. S., Ramakrishnan, C., and Varadarajan, R. (2003) *Protein Eng.* **16,** 187–193
28. Gossert, A. D., Bonjour, S., Lysek, D. A., Fiorito, F., and Wüthrich, K. (2005) *Proc. Natl. Acad. Sci. U.S.A.* **102,** 646–650
29. Sali, A., and Blundell, T. L. (1993) *J. Mol. Biol.* **234,** 779–815
30. Vakser, I. A., Matar, O. G., and Lam, C. F. (1999) *Proc. Natl. Acad. Sci. U.S.A.* **96,** 8477–8482
31. Mann, R., Mulligan, R. C., and Baltimore, D. (1983) *Cell* **33,** 153–159
32. Bestwick, R. K., Kozak, S. L., and Kabat, D. (1988) *Proc. Natl. Acad. Sci. U.S.A.* **85,** 5404–5408
33. Miller, A. D., and Buttimore, C. (1986) *Mol. Cell. Biol.* **6,** 2895–2902
34. Zahn, R., von Schroetter, C., and Wüthrich, K. (1997) *FEBS Lett.* **417,** 400–404
35. Hafner-Bratkovic, I., Gaspersic, J., Smid, L. M., Bresjanac, M., and Jerala, R. (2008) *J. Neurochem.* **104,** 1553–1564
36. Gaspersic, J., Hafner-Bratkovic, I., Stephan, M., Veranic, P., Bencina, M., Vorberg, I., and Jerala, R. (2010) *FEBS J.* **277,** 2038–2050
37. Bocharova, O. V., Breydo, L., Parfenov, A. S., Salnikov, V. V., and Baskakov, I. V. (2005) *J. Mol. Biol.* **346,** 645–659
38. Polymenidou, M., Moos, R., Scott, M., Sigurdson, C., Shi, Y. Z., Yajima, B., Hafner-Bratkovic, I., Jerala, R., Hornemann, S., Wuthrich, K., Bellon, A., Vey, M., Garen, G., James, M. N., Kav, N., and Aguzzi, A. (2008) *PLoS One* **3,** e3872
39. Bocharova, O. V., Breydo, L., Salnikov, V. V., Gill, A. C., and Baskakov, I. V. (2005) *Protein Sci.* **14,** 1222–1232
40. Kuwahara, C., Takeuchi, A. M., Nishimura, T., Haraguchi, K., Kubosaki, A., Matsumoto, Y., Saeki, K., Matsumoto, Y., Yokoyama, T., Itohara, S., and Onodera, T. (1999) *Nature* **400,** 225–226
41. Vorberg, I., Raines, A., Story, B., and Priola, S. A. (2004) *J. Infect. Dis.* **189,** 431–439
42. Maas, E., Geissen, M., Groschup, M. H., Rost, R., Onodera, T., Schätzl, H., and Vorberg, I. M. (2007) *J. Biol. Chem.* **282,** 18702–18710
43. Ertmer, A., Gilch, S., Yun, S. W., Flechsig, E., Klebl, B., Stein-Gerlach, M., Klein, M. A., and Schätzl, H. M. (2004) *J. Biol. Chem.* **279,** 41918–41927
44. Polymenidou, M., Stoeck, K., Glatzel, M., Vey, M., Bellon, A., and Aguzzi, A. (2005) *Lancet Neurol.* **4,** 805–814
45. Kaneko, K., Zulianello, L., Scott, M., Cooper, C. M., Wallace, A. C., James, T. L., Cohen, F. E., and Prusiner, S. B. (1997) *Proc. Natl. Acad. Sci. U.S.A.* **94,** 10069–10074
46. Guo, Z., and Eisenberg, D. (2006) *Proc. Natl. Acad. Sci. U.S.A.* **103,** 8042–8047
47. DeMarco, M. L., and Daggett, V. (2007) *Biochemistry* **46,** 3045–3054
48. Kocisko, D. A., Priola, S. A., Raymond, G. J., Chesebro, B., Lansbury, P. T., Jr., and Caughey, B. (1995) *Proc. Natl. Acad. Sci. U.S.A.* **92,** 3923–3927
49. Hunter, N., Goldmann, W., Benson, G., Foster, J. D., and Hope, J. (1993) *J. Gen. Virol.* **74,** 1025–1031
50. Sigurdson, C. J., Nilsson, K. P., Hornemann, S., Heikenwalder, M., Manco, G., Schwarz, P., Ott, D., Rülicke, T., Liberski, P. P., Julius, C., Falsig, J., Stitz, L., Wüthrich, K., and Aguzzi, A. (2009) *Proc. Natl. Acad. Sci. U.S.A.* **106,** 304–309
51. Lührs, T., Zahn, R., and Wüthrich, K. (2006) *J. Mol. Biol.* **357,** 833–841
52. Tattum, M. H., Cohen-Krausz, S., Thumanu, K., Wharton, C. W., Khalili-Shirazi, A., Jackson, G. S., Orlova, E. V., Collinge, J., Clarke, A. R., and Saibil, H. R. (2006) *J. Mol. Biol.* **357,** 975–985
53. Kaimann, T., Metzger, S., Kuhlmann, K., Brandt, B., Birkmann, E., Holtje, H. D., and Riesner, D. (2008) *J. Mol. Biol.* **376,** 582–596
54. Stöhr, J., Weinmann, N., Wille, H., Kaimann, T., Nagel-Steger, L., Birkmann, E., Panza, G., Prusiner, S. B., Eigen, M., and Riesner, D. (2008) *Proc. Natl. Acad. Sci. U.S.A.* **105,** 2409–2414
55. Staniforth, R. A., Giannini, S., Higgins, L. D., Conroy, M. J., Hounslow, A. M., Jerala, R., Craven, C. J., and Waltho, J. P. (2001) *EMBO J.* **20,** 4774–4781
56. Sambashivan, S., Liu, Y., Sawaya, M. R., Gingery, M., and Eisenberg, D. (2005) *Nature* **437,** 266–269
57. Yamasaki, M., Li, W., Johnson, D. J., and Huntington, J. A. (2008) *Nature* **455,** 1255–1258
58. Knaus, K. J., Morillas, M., Swietnicki, W., Malone, M., Surewicz, W. K., and Yee, V. C. (2001) *Nat. Struct. Biol.* **8,** 770–774
59. Lee, S., Antony, L., Hartmann, R., Knaus, K. J., Surewicz, K., Surewicz, W. K., and Yee, V. C. (2010) *EMBO J.* **29,** 251–262
60. Welker, E., Raymond, L. D., Scheraga, H. A., and Caughey, B. (2002) *J. Biol. Chem.* **277,** 33477–33481
61. Turk, E., Teplow, D. B., Hood, L. E., and Prusiner, S. B. (1988) *Eur. J. Biochem.* **176,** 21–30
62. Cordeiro, Y., Machado, F., Juliano, L., Juliano, M. A., Brentani, R. R., Foguel, D., and Silva, J. L. (2001) *J. Biol. Chem.* **276,** 49400–49409
63. Deleault, N. R., Harris, B. T., Rees, J. R., and Supattapone, S. (2007) *Proc. Natl. Acad. Sci. U.S.A.* **104,** 9741–9746
64. Silva, J. L., Lima, L. M., Foguel, D., and Cordeiro, Y. (2008) *Trends Biochem. Sci.* **33,** 132–140
65. Caughey, B., and Raymond, G. J. (1993) *J. Virol.* **67,** 643–650
66. Vieira, T. C., Reynaldo, D. P., Gomes, M. P., Almeida, M. S., Cordeiro, Y., and Silva, J. L. (2011) *J. Am. Chem. Soc.* **133,** 334–344
67. Makarava, N., and Baskakov, I. V. (2008) *J. Biol. Chem.* **283,** 15988–15996
68. Colby, D. W., Giles, K., Legname, G., Wille, H., Baskakov, I. V., DeArmond, S. J., and Prusiner, S. B. (2009) *Proc. Natl. Acad. Sci. U.S.A.* **106,** 20417–20422
69. Shindoh, R., Kim, C. L., Song, C. H., Hasebe, R., and Horiuchi, M. (2009) *J. Virol.* **83,** 3852–3860
70. Wiltzius, J. J., Landau, M., Nelson, R., Sawaya, M. R., Apostol, M. I., Goldschmidt, L., Soriaga, A. B., Cascio, D., Rajashankar, K., and Eisenberg, D. (2009) *Nat. Struct. Mol. Biol.* **16,** 973–978